An Integrated Neighborhood Correlation and Hierarchical Clustering Approach of Functional MRI

Huafu Chen, Hong Yuan, Dezhong Yao*, Lin Chen, and Wufan Chen

***Abstract*—Clustering analysis is a promising data-driven method for the analysis of functional magnetic resonance imaging (fMRI) time series, however, the huge computation load makes it difficult for practical use. In this paper, neighborhood correlation (NC) and hierarchical clustering (HC) methods are integrated as a new approach where fMRI data are processed first by NC to get a preliminary image of brain activations, and then by HC to remove some noises. In HC, to better use spatial and temporal information in fMRI data, a new spatio-temporal measure is introduced. A simulation study and an application to visual fMRI data show that the brain activations can be effectively detected and that different response patterns can be discriminated. These results suggest that the proposed new integrated approach could be useful in detecting weak fMRI signals.**

***Index Terms*—fMRI, hierarchical clustering analysis, neighborhood correlation, spatio-temporal measure.**

I. Introduction

FUNCTIONAL magnetic resonance imaging (fMRI) has emerged as a useful tool in the study of brain function. This imaging modality utilizes the fact that the MRI signal is sensitive to some hemodynamic parameters that change during neuronal activation (e.g., blood flow, blood volume, and oxygenation). The changes of these parameters cause small intensity fluctuation of a properly weighted MR images. The blood oxygenation level-dependent (BOLD) contrast-based imaging method is the most commonly employed in current fMRI. BOLD contrast is dependent on a decrease of local deoxyhemoglobin concentration in an area of neuronal activation [1], [2]. This local decrease in paramagnetic material increases the apparent transverse relaxation constant, resulting in an increase of MR signal intensity in the area affected. Other methods of functional MR imaging contrast include measurement of cerebral blood flow and volume effects [3].

Some researchers have attempted to address the fMRI data processing issue by using parametric methods [4], [5]. The parametric methods usually assume specific signal shapes (Poisson, Gaussian, Gamma, etc.) and attempt to extract the associated parameters for which the data are fit best. One such method, the widely used statistical parametric mapping (SPM), is a general linear model-based method [6], [7]. A drawback of such model-driven methods is that it requires prior experimental information and hypothesis about the paradigm. Meanwhile, exploratory data-driven analysis, such as principal components analysis and independent components analysis (ICA), does not require prior experimental information and hypothesis about the paradigm or the hemodynamic response function, and they are now also widely used by many groups [8]–[11]. A problem with these data-driven approaches is the choice of meaningful decomposed components. Recently, another class of fMRI analysis method, the clustering methods (CM), [12]–[15] have become popular as well. The main drawback is the so-called ill-balanced data problem [12], [16], i.e., the activated regions are a small proportion of the brain and they are embedded in the mass of nonactivities voxels. Handling such a problem by CM itself is not easy. Furthermore, the physiological interpretation of the cluster is not straightforward.

Comparing various clustering methods, we found that the definition of distance between two time series is the determinant factor of a clustering analysis [9]–[12], [17], [18]. There are two main shortcomings of clustering methods, one is the stability when the noise level is high; the second is a resource problem because a fMRI slice of 128×128 voxels with 80 temporal points will produce a clustering matrix of $16\,384 \times 16\,384$. Due to the limited resource of a computer, it is impossible to run this method on a general computer at present.

In general, the clustering method may be based on the original fMRI data, thus, it may be classified as a data-driven method [19]–[24], it may also be based on the cross-correlation value between the fMRI data and the stimulus [12], then it is a model-driven method with requirement of the experimental information. Typically, as brain activations evoked by various stimuli are not manifested as a single voxel, but rather as groups of tens to hundreds of voxels [22], [23], [34]. The correlations between each activated voxel and its neighboring activated voxels should

Manuscript received January 28, 2005; revised June 11, 2005. This work was supported in part by the National Basic Research Program (973) of China under Project 2003CB716100, in part by the National Science Foundation of China (NSFC) under Grant 90208003, Grant 30130180, and Grant 30200059, and in part by the Doctor training Fund of MOE, PRC, Fok Ying Tong Education Foundation (91041), Middle-youth academic leader training plan of UESTC. *Asterisk indicates corresponding author.*

H. Chen is with the Center of Neuroinformatics, School of Life Science and Technology, School of Applied Math, University of Electronic Science and Technology of China, Chengdu 610054, China. He is also with the Key Laboratory of Cognitive Science, Graduate School and Institute of Biophysics, Chinese Academy of Science 100101, China (e-mail: chenhf@uestc.edu.cn).

H. Yuan is with the Center of Neuroinformatics, School of Life Science and Technology, School of Applied Math, University of Electronic Science and Technology of China, Chengdu 610054, China.

*D. Yao is with the Center of Neuroinformatics, School of Life Science and Technology, School of Applied Math, University of Electronic Science and Technology of China, Chengdu 610054, China (e-mail: Dyao@uestc.edu.cn).

L. Chen is with the Key Laboratory of Cognitive Science, Graduate School and Institute of Biophysics, Chinese Academy of Science 100101, China.

W. Chen is with the Center of Neuroinformatics, School of Life Science and Technology, School of Applied Math, University of Electronic Science and Technology of China, Chengdu 610054, China. He is also with the School of Biomedical Engineering Southern Medical University, Guangzhou 510515, China.

Digital Object Identifier 10.1109/TBME.2005.869660

be high while the correlations between an activated voxel and its neighboring nonactivated voxels should be low.

In this paper, our goal is to develop a data-driven clustering method implemented on a personal computer. In order to reduce the computation complexity, a neighborhood correlation (NC) is utilized at first to get a primary image, here the neighborhood idea just follows the tiny domain idea in our previous tiny domain ICA algorithm [24]. A HC method is further applied to the dimension reduced primary imaging result to get the final imaging result. In our HC procedure, a new spatio-temporal measure is introduced. NC and HC methods are introduced in Section II. Simulation data and fMRI experiments are presented in Section III. The simulation and real fMRI results are discussed in Sections IV and V.

II. Methods and Data

A. NC Approach

The maximum of the correlation coefficients (CCs) between voxel k and its neighborhood voxels can be computed as follows:

$$\mathrm{CC}_k = \max_{j \in K, j \neq k} \{\mathrm{corr}(v_k, v_j)\} \tag{1}$$

where the set K is composed of voxels neighboring to Voxel k except the voxel k, $corr(v_k, v_j)$ is the normalized CCs between the time sequences of voxel k (v_k) and voxel j (v_j).

In our practice, CCs between each voxel and its four neighborhoods are calculated, and the maximum CC is saved. Finally obtained is a map with each point denoted the maximum CC. Choosing a threshold that most of the voxels are eliminated, and the remaining voxels are supposed to be candidates of the actual active voxels. We consider this result as a preliminarily imaging result because it still suffers from some noises effect. For example, if there is intense and similar noises cover an area larger than two voxels, a relative large CC may be generated and the voxel will be wrongly selected as a possible active voxel. To prevent such errors, HC is introduced for further analysis as below.

B. HC Approach

The idea of HC can be shown by a biological classification in Fig. 1 [25]. In biology, clustering data uses the taxonomic hierarchies. Plants or animals are grouped in species, which in turn are grouped in genera, then families, orders, classes, and finally phyla. Each level of the taxonomy gathers several members of the previous level.

The key factor impacting the performance of HC is the distance measure. The conventional measurement of the distance between two spatial positions is the Euclidean distance d_{Es}

$$d_{\mathrm{Es}} = \sqrt{(x_i - x_j)^2 + (y_i - y_j)^2} \tag{2}$$

where (x_i, y_i) and (x_j, y_j) represent the coordinates of voxel v_i and v_j, respectively. In this paper, the coordinate value (x_i, y_i) of a voxel v_i is defined as the normalized order number by the dimension size of the image, thus, $0 \leq x_i \leq 1, 0 \leq y_i \leq 1$. The distance between the time series of two voxels can be defined as

$$d_{\mathrm{Et}} = \sqrt{\sum_{k=1}^{N} (t_{ik} - t_{jk})^2} \tag{3}$$

where t_{ik} is the value of voxel v_i at the time point k, N is the number of samples.

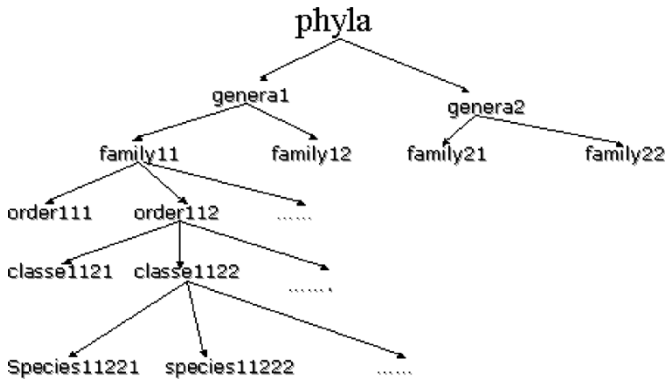

Fig. 1. Illustration of HC.

As a fMRI data is a spatio-temporal information dataset, we defined a new measure of the spatio-temporal distance between two voxels as

$$d_{\mathrm{ST}} = (1 - \mathrm{corr}(v_i, v_j)) \times e^{(|x_i - x_j| + |y_i - y_j|)} \tag{4}$$

where $D_S = |x_i - x_j| + |y_i - y_j|$ is the L1 norm spatial distance between voxel v_i and v_j, $0 \leq D_S \leq 2$; $Cor = corr(v_k, v_j)$ is the normalized CCs between the time sequences of voxel v_i and voxel v_j. The measure is based on the physiological fact that spatially close neighborhoods and temporally correlated activations are the most likely actual activations. Fig. 2 shows the spatio-temporal measure for an image with dimension 128 $\times$ 128. Where the two axes are the L1 norm spatial distance and the temporal correlation of two voxels, the closer in space and more similar in temporal sequences, the smaller the spatio-temporal distance.

C. Synthetic Data Generation

In this paper, a synthetic fMRI image (128 $\times$ 128 voxels) is generated on an axial brain as shown Fig. 3. Fig. 3(a) is composed of five active subregions (471 voxels) with a time invariant margin of 8790 voxels and a stochastic variant texture of 4594 voxels (gray/white matter, ventricles). The five subregions are different in size, shape, temporal process, and signal-to-noise ratio (SNR) (SNR is defined as the standard deviation ratio between noise and signal). The time series of all the voxels of a subregion consist of a certain signal mixed with Gaussian noise as shown in Fig. 3(c). The supposed box-car-like signals are shown in Fig. 3(b). The signal 1 in Fig. 3(b) is a practical stimulus pattern used in the following actual fMRI data collection, and it is used here for subregions A and E with a common 5-s delay, but the $\mathrm{SNR} = 20\%$ and 10% for A and E, respectively in Fig. 3(c). Signal 1 is also used for subregion D with a 2-s delay and $\mathrm{SNR} = 10\%$ as shown in Fig. 3(c). subregions B and C are activated by a smoothed pattern signal, signal 2 in Fig. 3(b), the SNRs are 20% and 1% for B and C in Fig. 3(c),

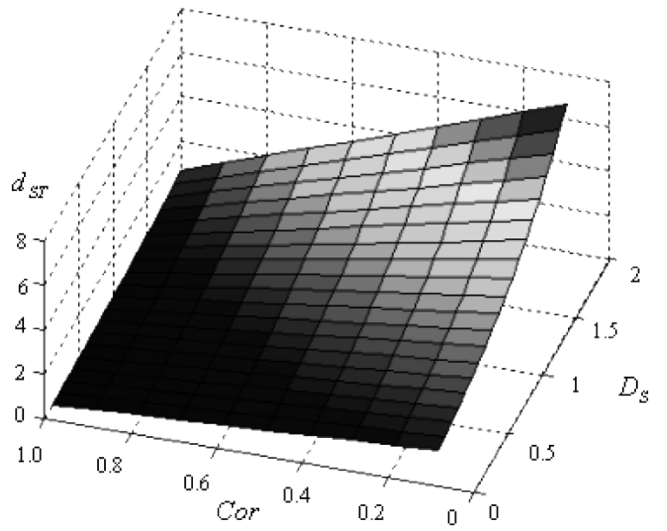

Fig. 2. Spatio-temporal distance measure. The vertical axis is the distance measure d_{ST}, the two lateral axis are the temporal Cor between two voxels and the L1 norm spatial distance D_{S} of two voxels.

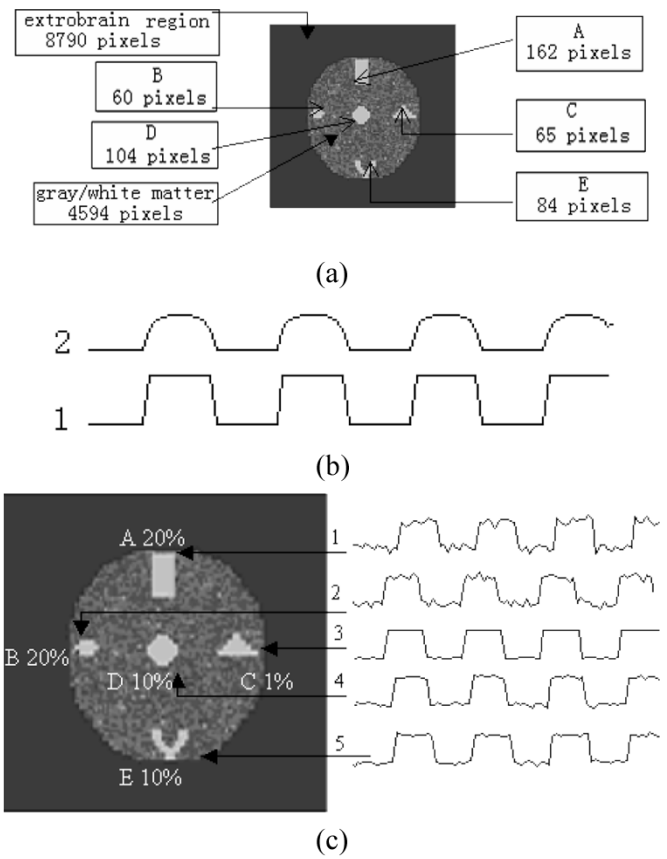

Fig. 3. Synthetic fMRI image. (a) Spatial distribution of assumed active voxels; (b) assumed box-car-like stimulation pattern with 10 points at rest and 10 points at task conditions, respectively; (c) temporal patterns of the five assumed active subregions.

respectively. The relative delays between B and C, C and signal 1 in Fig. 3(b) are all 2s.

D. Experimental Paradigm

The stimuli consist of circular black-and-white checkerboards (the checkerboards subtend $10'$ of arc), each stimulus with a 2° diameter visual angle and a spatial frequency of 3.2 cycles/°. Stimuli pattern is the block design, signal 1 in Fig. 3(b), each stimulus was presented for 50 ms. These stimuli were presented randomly in the left and right visual fields (VFs) (stimulus onset asynchronies (SOAs) varying from 250 to 500 ms) in 20-s trials. After the stimuli were presented to the left and right VFs, a blank trial was followed. In this blank trial, only the center fixation cross (0.8°) was displayed. Subjects were required to concentrate on the fixation cross and press a button upon detection of an infrequent brightness change of the fixation cross [26], [27].

In our fMRI experiments, eight normal subjects were involved in the above visual task with a block paradigm. Experiment was conducted at Beijing hospital MRI center with SIEMENS 1.5 TESLA MAGNETOM TRIO. EPI: repetition time $\mathrm{TR} = 2.0$ s, matrix size $= 128 \times 128$, $\mathrm{TE} = 50$ ms, flip angle 90°. The first 4 scans of each run were discarded to allow for magnetic saturation effects. Then 80 volume images comprised time-series were analyzed.

E. Procedure of the Data Processing

First, the fMRI data were motion corrected, spatially smoothed with a 12-mm 3 full-width at half-maximum Gaussian kernel, spatially normalized into the standard Montreal Neurological Institute space by SPM99 (Http://www.fil.ion.ucl.uk/spm/spm99) and all voxels outside brain area are removed. Second, the data is processed by NC, and then by HC.

III. Results

A. Simulation Test

1) NC Approach: In this section, the validity of NC is evaluated. The size of the simulation data, shown in Fig. 4, is $128 \times 128 \times 80$. It's impossible to analyze such a huge dataset directly by HC, which requires huge memory and heavy computation of the dissimilarity matrix. Fig. 4(a) shows the signal distribution of one time point. The CC distribution of NC is shown in Fig. 4(b). By using a CC threshold 0.3, we get 602 possible active voxels (471 actual activated points and 131 noise points) as shown in Fig. 4(c). The remaining 602 voxels are much less than the original 128×128 voxels. Apparently, NC is successful in picking up those voxels that we interested in as well as deleting the most irrelevant voxels, and reducing the calculation complexity largely for the following HC.

2) HC: The data presented above in Fig. 4(c) is further processed with the HC algorithm. Based on the spatio-temporal distance d_{ST} (4), the HC results are shown in Fig. 5. The cluster in Fig. 5(c) is specified as the meaningful cluster for the high CC (0.86) between the average time signal of all voxels in this cluster and the stimulation pattern shown in Fig. 3. The other two clusters in Fig. 5(a),(b) are specified as nonmeaningful noise patterns for their CCs, 0.09 and 0.089, are much smaller than the above 0.86

To further separate the different response patterns, the remaining data shown by Fig. 5(c) is further hierarchically processed with HC. Three clusters in Fig. 6(a)–(c) are specified as the meaningful three clusters based on their high CCs:0.91,

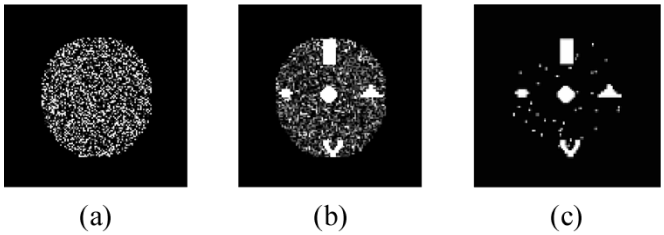

Fig. 4. Result of NC. (a) Synthetic pattern at one single time point; (b) distribution of the NC coefficient; (c) imaging result of NC with a threshold 0.3.

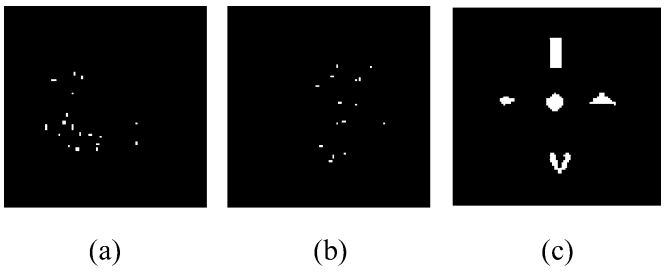

Fig. 5. Result of HC. (a) and (b) Two noise patterns; (c) activation pattern.

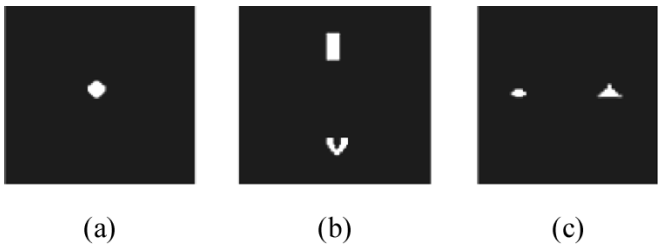

Fig. 6. Simulation result. (a) Activation region corresponding to the forth signal shown in Fig. 3(c); (b) activation regions corresponding to the first and fifth signal pattern shown in Fig. 3(c); (c) activation regions corresponding to the second and third signals shown in Fig. 3(c).

0.87 and 0.89, respectively. It is reasonable to see that each of new clusters has a larger CC than their average case (0.86) shown by Fig. 5(c). Fig. 6(a) shows the region D with 104 voxels corresponding to the forth signal in Fig. 3(c). Fig. 6(b) shows regions A and E with $162+84 = 246$ voxels corresponding to the first and fifth signals in Fig. 3(c); Fig. 5(c) illustrates regions B and C with $60 + 65 = 125$ voxels corresponding to the second and third signals in Fig. 3(c).

B. Actual Visual fMRI Experiment Data Test

1) NC: The fMRI data is analyzed by NC, and the result is shown in Fig. 7, where 180 voxels are remained by a threshold 0.3.

2) HC: By HC, the 180 voxels are clustered into two groups as shown in Fig. 8. One cluster contains 101 voxels spreading the whole brain as shown in Fig. 8(a), the average time series of these 101 voxels is shown in Fig. 8(b). The small CC 0.1241 between the signal in Fig. 8(b) and the experiment paradigm indicates these points are nonactivation voxels, thus, it is not specified as a meaningful cluster. Another cluster contains 79 voxels mostly located in the visual cortex as shown in Fig. 8(c), the average time series signal of these 79 voxels is show in Fig. 8(d), it is highly correlated with the experiment paradigm, $\mathrm{CC} = 0.6237$, thus, specified as a meaningful cluster. Using

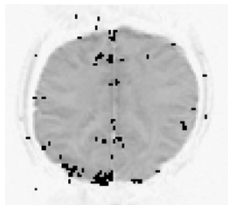

Fig. 7. Result of NC. The black points are the potential activation points chosen by a threshold 0.3.

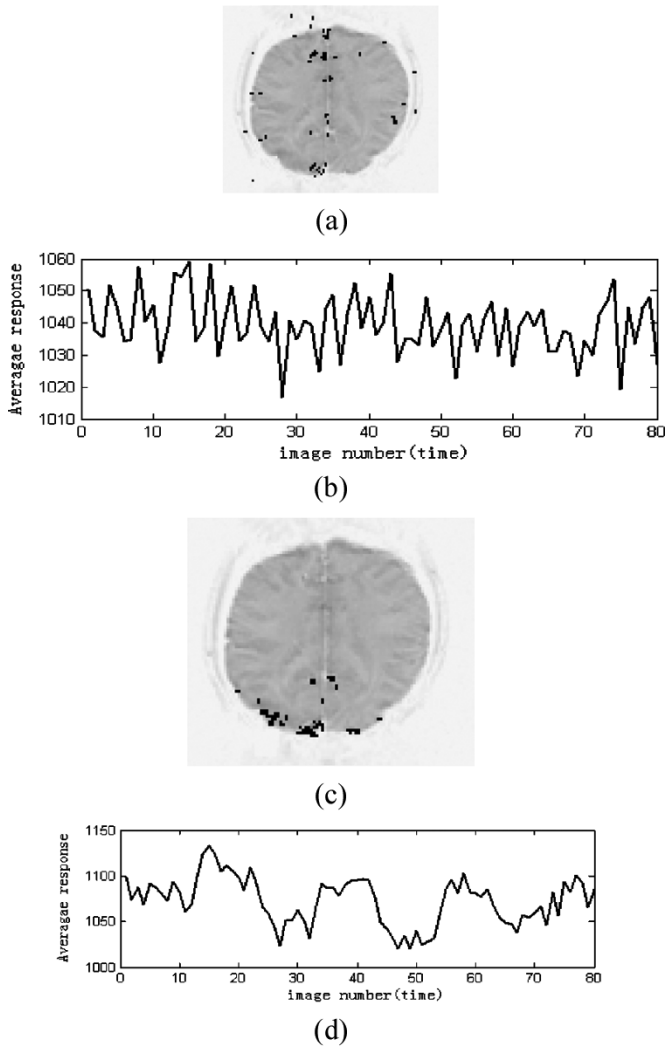

Fig. 8. Clustering result. The black points are activation points. (a) Cluster one, (b) average time series corresponding to (a); (c) cluster two, (d) average time series corresponding to (c).

the same method, the clustering results of the other two slices are shown in Fig. 9. Figs. 8(c) and 9 show that the excited areas evoked by a visual stimulation are mainly located in the region of the primary visual cortex.

3) SPM Result: Fig. 10 shows the fMRI imaging result map using the public-domain SPM software (http://www.fil.ion.ucl.ac.uk/) where the significance threshold for statistical parametric maps is $\mathrm{P} < 0.05$. The main aspects of Figs. 8(c), Fig. 9, and 10 are consistent that both methods confirm that the excited areas evoked by a visual stimulus are mainly located in the region of the primary visual cortex.

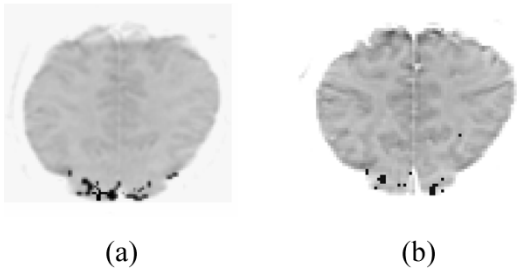

Fig. 9. Clustering result of two other slices. The black points are activation points.

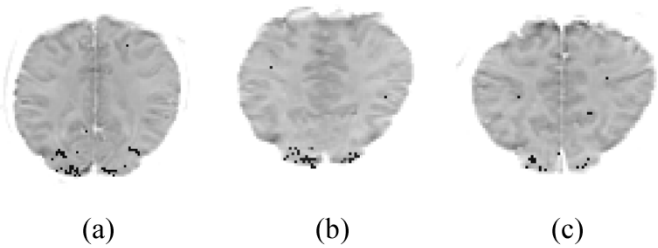

Fig. 10. Result of $\mathrm{SPM}(\mathrm{p} = 0.05)$. (a) Slice corresponding to Fig. 8(c); (b), (c) Other two slices corresponding to Fig. 9. Black points are activation points.

However, the new method give more clustered voxels, and the computation is more efficient because the remaining voxels after the easily implemented NC is really limited, thus, quite different from SPM processed voxel by voxel over all the voxels.

C. Detailed Result of the Actual Visual fMRI Experiment Data

Figs. 8(a) and 9 show the brain activation voxels evoked by the visual stimuli. To detect various responses to a stimulation task, Fig. 8(c) is further analyzed by HC. Fig. 11 shows the result, where Fig. 11(a)–(c) shows three clusters of activation voxels in Fig. 8(c). Fig. 11(d)–(f) shows the fMRI signals of the activation voxels corresponding to Fig. 11(a)–(c). Delay correlation is computed between the signals in Fig. 11(d)–(f) and the experiment pattern shown by signal 1 in Fig. 3(b), respectively. The maximum CCs of Fig. 11(d)–(f) are 0.8402, 0.8279, and 0.7451 with 2, 3, and 4 sample points delay, respectively. These three clusters are all specified as meaningful clusters. These facts mean that the BOLD dynamic responses of various local brain regions are different in both response pattern and delay, and this information may be very helpful in further detail study of the brain information process, such as the spatio-temporal connectivity of the fMRI data [17]. Apparently, such a further detailed segregation ability of HC is a distinct priority over the SPM.

IV. Discussion

A. The Difference of the Dynamic Responses

The results in Fig. 11 show that the dynamic waveforms of the BOLD signals in different occipital lobe regions are distinctly different from each other, consistent with our prior ICA and model studies [27]–[29]. If comparing with the stimulus pattern, signal 1 in Fig. 3(b), these dynamic responses are clearly nonlinear, and all these facts provide us chance to analyze the temporal dynamic process and spatial connectivity of a fMRI data,

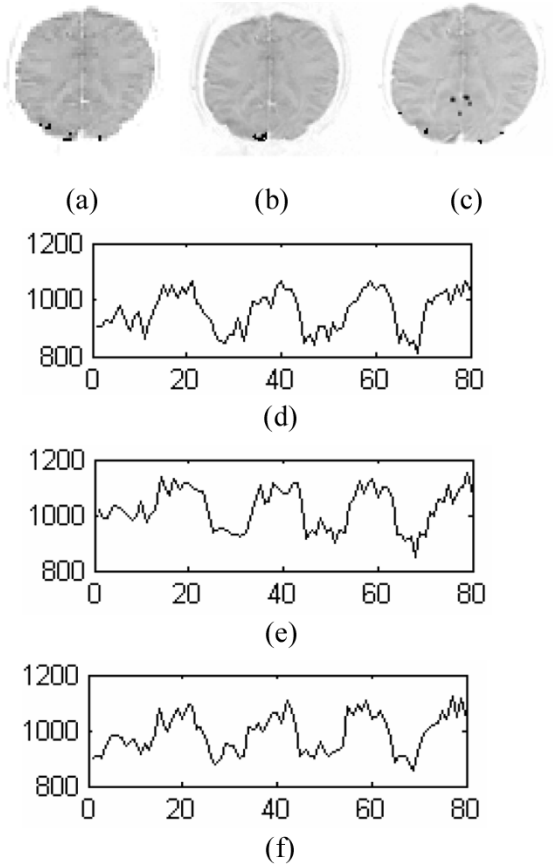

Fig. 11. HC imaging results of Fig. 8(b). (a)–(c) Three spatial clusters decomposed of Fig. 8(b); (d)–(f) The fMRI signals of the activation voxels correspond to (a)–(c).

further more, combing the time delay information and stimulus task related neuro-anatomical knowledge, even more information than the imaging map may be obtained.

B. Distance Measure Selection

For comparison, the following Euclidean distance d_{Est} is checked:

$$d_{\mathrm{Est}} = \sqrt{(x_i - x_j)^2 + (y_i - y_j)^2 + \sum_{k=1}^{N} (t_{ik} - t_{jk})^2} \quad (5)$$

where x_i and y_i are the coordination of voxel v_i, t_{ik} is the time series value of v_i at a time point k, and N is the number of time points. Replaced the prior spatio-temporal distance d_{ST} by the Euclidean distance d_{Est} and kept all the other conditions, the algorithm failed to cluster the regions in Fig. 3 into three different patterns. This fact means that d_{ST} is better than the simply Euclidean distance measure d_{Est} in denoting the similarity of two voxels in fMRI when we need to take the spatial and temporal information into consideration at the same time.

When simply considering the temporal information by using the Euclidean distance $\mathrm{d_{Et}}$ instead of the spatio-temporal distance d_{ST}, the algorithm can cluster the five regions in Fig. 3 into three patterns successfully. However, if the data are mixed with some noise $(\mathrm{SNR} > 1\%)$, it fails to separate noises from activation points.

These results suggest Euclidean distance measures $\mathrm{d_{Et}}$ and d_{Est} are not good distance measure in characterizing the similarities of two fMRI voxels. Contrastingly, our new spatio-temporal distance measure successful categorized all points into activation regions and noises as shown in Fig. 5. The above results show that all the noise voxels are separated from active voxels, and signals of different patterns are separated as illustrated in Fig. 6 by our HC.

C. Threshold Selection of NC

In general, NC alone may be an imaging method, and the CC map seems to depend on the noise acquired along with the fMRI signals, so the threshold for a NC process should be based on the statistical difference ($\mathrm{p} < 0.05$ or 0.01, etc.) between chosen voxels and nonchosen voxels. In this paper, NC is assumed just to provide a primary map for the following HC, thus, we hope that almost all the real active voxels remained even some noisy voxels are wrongly selected. Based on this concern, a statistical difference $(\mathrm{p} < 0.1)$ is taken in our work, and the corresponding actual threshold is about 0.3 in our work.

D. Limitation of the Method

The result in Fig. 6 shows that regions A and E are classified into one cluster, though they have different noise levels 20% and 10%. Regions B and C are classified into another although they are of different noise levels 20% and 1%. D is classified into one cluster. These facts mean the algorithm mainly takes account of signal patterns and time delays but not noise levels, or say it is sensitive to signal patterns and time delays and is robust to noise. Our simulation tests show that the method may fail only for large SNR such as >80%. Meanwhile, if there are strongly spatio-temporal correlated noises such as possible various physiological pulsations, the method also may fail or make the explanation complicated. Besides, the choice of the NC threshold needs careful consideration, a small value will reduce the computation efficiency, and a large value may lose some meaningful active points, and our opinion is to do the choice according to the statistical difference between chosen voxels and nonchosen voxels as noted above.

V. Conclusion

In this paper, we proposed an integration method of NC and HC to detect brain activations. The validity of this algorithm was tested by simulation study and real fMRI data. The results show that the various brain activation points can be effectively detected, and different response patterns can be separated by the NC-HC integrated algorithm.

References

[1] S. Ogawa, T. M. Lee, A. R. Kay, and D. W. Tank, "Brain magnetic resonance imaging with contrast dependent on blood oxygenation," *Proc. Nat. Acad. Sci.*, vol. 87, pp. 9868–9872, 1990.

[2] K. K. Kwong, J. W. Belliveau, D. A. Chesler, I. E. Goldberg, R. M. Weisskoff, B. P. Poncelet, D. N. Kennedy, B. E. Hoppel, M. S. Cohen, R. Turner, H. Cheng, T. J. Brady, and B. R. Rosen, "Dynamic magnetic resonance imaging of human brain activity during primary sensory stimulation," *Proc. Nat. Acad. Sci.*, vol. 89, pp. 5675–5679, 1992.

[3] J. W. Belliveau, D. N. Kennedy, R. C. McKinstry, B. R. Buchbinder, R. M. Weisskoff, M. S. Cohen, J. M. Vevea, T. J. Brady, and B. R. Rosen, "Functional mapping of the human visual cortex by magnetic resonance imaging," *Science*, vol. 254, pp. 716–719, 1991.

[4] F. Kruggel and D. Y. von Cramon, "Temporal properties of the hemody-namic response in functional MRI," *Hum. Brain Mapp.*, vol. 8, pp. 259–271, 1999.

[5] V. Solo, P. Purdon, R. Weisskoff, and E. Brown, "A signal estimation approach to functional MRI," *IEEE Trans. Med. Imag.*, vol. 20, no. 1, pp. 26–35, Jan. 2001.

[6] K. J. Friston, P. Jezzard, and R. Turner, "Analysis of functional MRI time-series," *Hum. Brain Mapp.*, vol. 2, pp. 69–78, 1994.

[7] K. J. Worsley and K. J. Friston, "Analysis of fMRI time-series revisited—again," *NeuroImage*, vol. 2, no. 1, pp. 173–181, 1885.

[8] J. J. Sychra, P. A. Bandettini, N. Bhattacharya, and Q. Lin, "Synthetic images by subspace transforms I. Principal components images and related filters," *Med. Phys.*, vol. 21, no. 2, pp. 193–201, 1994.

[9] W. Backfrieder, R. Baumgartner, M. Samal, E. Moser, and H. Bergmann, "Quatification of I intensity variations in functional MR images using rotated principal components," *Phys. Med. Biol.*, vol. 41, pp. 1425–1438, 1996.

[10] M. J. McKeown, S. Makeig, G. G. Brown, T.-P. Jung, S. S. Kindermann, A. J. Bell, and T. J. Sejnowski, "Analysis of fMRI data by blind separation into independent spatial components," *Hum. Brain Mapp.*, vol. 6, pp. 160–188, 1998.

[11] M. J. McKeown, T.-P. Jung, S. Makeig, G. Brown, S. S. Kindermann, T.-W. Lee, and T. J. Sejnowski, "Spatially independent activity patterns in functional MRI data during the Stroop color-naming task," *Proc. Nat. Acad. Sci.*, vol. 95, pp. 803–810, 1998.

[12] C. Goutte, P. Toft, E. Rostrup, F. A. Nielsen, and L. K. Hansen, "On clustering fMRI time series," *NeuroImage*, vol. 9, pp. 298–310, 1999.

[13] K.-H. Chuang, M.-J. Chiu, C.-C. Lin, and J.-H. Chen, "Model-free functional MRI analysis using Kohonen clustering neural network and fuzzy c-means," *IEEE Trans. Med. Imag.*, vol. 18, no. 12, pp. 1117–1128, Dec. 1999.

[14] A. Baune, F. T. Sommer, M. Erb, D. Wildgruber, B. Kardatzki, G. Palm, and W. Grodd, "Dynamical cluster analysis of cortical fMRI activation," *NeuroImage*, vol. 9, pp. 477–489, 1999.

[15] S. Chen, C. A. Bouman, and M. Lowe, "Clustered components analysis for functional MRI," *IEEE Trans. Med. Imag.*, vol. 23, no. 1, pp. 85–98, Jan. 2004.

[16] J. C. Bezdek, *Pattern Recognition With Fuzzy Objective Functions Agorithms*. New York: Plenum, 1981.

[17] F. G. Meyer and J. Chinrungrueng, "Spatiotemporal clustering of fMRI time series in the spectral domain," *Med Image Anal.*, vol. 9, no. 1, pp. 51–68, Feb. 2005.

[18] E. Dimitriadou, M. Barch, and C. Windischberger *et al.*, "A quantitative comparison of functional MRI cluster analysis," *Artif. Intell. Med.*, vol. 31, pp. 57–71, 2004.

[19] R. Baumgartner, L. Ryner, W. Richter, R. Summers, M. Jarmasz, and R. Somorjai, "Comparison of two exploratory data analysis methods for fMRI: fuzzy clustering vs. principal component analysis," *Magn. Reson. Imag.*, vol. 18, pp. 89–94, 2000.

[20] R. Baumgartner, G. Scarth, C. Teichtmeister, R. Somorjai, and E. Moser *et al.*, "Fuzzy clustering of gradient-echo functional MRI in the human visual cortex. Part I: reproducibility," *J. Magn. Reson. Imag.*, vol. 7, no. 6, pp. 1094–1101, 1997.

[21] S. Hayasaka and T. E. Nichols, "Validating cluster size inference: random field and permutation methods," *NeuroImage*, vol. 20, no. 4, pp. 2343–2356, 2003.

[22] Y. Lu, T. Jiang, and Y. Zang, "A split-merge-based region-growing method for fMRI activation detection," *Hum. Brain Mapp.*, vol. 22, no. 4, pp. 271–279, 2004.

[23] Y. Zang, T. Jiang, Y. Lu, Y. He, and L. Tian, "Regional homogeneity approach to fMRI data analysis," *Neuroimage*, vol. 22, no. 1, pp. 2:394–2:400, 2004.

[24] H. Chen, D. Yao, Y. Zhuo, and L. Chen, "Analysis of fMRI data by blind separation into independent temporal component," *Brain Topogr.*, vol. 15, no. 4, pp. 223–232, 2003.

[25] B. D. Ripley, *Pattern Recognition and Nerual Networks*. Cambridge, U.K.: Cambridge Univ. Press, 1996.

[26] F. Di Russo, A. Martínez, M. Sereno, S. Pitzalis, and S. A. Hillyard, "Cortical sources of the early components of the visual evoked potential," *Hum. Brain Mapp.*, vol. 15, pp. 95–111, 2001.

[27] H. Chen, D. Yao, and Z. Liu, "A study on asymmetry of spatial visual field by analysis of the fMRI BOLD response," *Brain Topogr.*, vol. 17, no. 1, pp. 39–46, 2004.

[28] H. Chen and D. Yao, "Discussion on the choice of separation component in fMRI data analysis by spatial independent component analysis," *Magn. Reson. Imag.*, vol. 22, no. 6, pp. 827–833, 2004.

[29] H. Chen, D. Yao, and Z. Liu, "A comparison of Gamma and Gaussian dynamic convolution models of the fMRI BOLD response," *Magn. Reson. Imag.*, vol. 23, pp. 83–88, 2005.

Huafu Chen received the Ph.D. degree in biomedical engineering from the University of Electronic Science and Technology of China (UESTC), Chengdu, China, in 2004.

He is the author or coauthor of more than 50 scientific papers. He is currently a Professor in the School of Life Science and Technology, UESTC. His major research interests include independent component analysis, functional magnetic resonance imaging, and signal and image processing.

Hong Yuan received the MS degree in biomedical engineering from the University of Electronic Science and Technology of China (UESTC), Chengdu, China, in 2005.

She is now a faculty member of the School of Psychology of Southwest Normal University, ChongQing, China. Her research interest is biomedical signal processing; especially fMRI and EEG.

Dezhong Yao received the Ph.D. degree in applied geophysics from Chengdu University of Technology, Chengdu, China, in 1991, and completed the postdoctoral fellowship in electromagnetic field at the University of Electronic Science and Technology of China (UESTC), Chengdu, China, in 1993.

He has been a faculty member since 1993; a Professor since 1995; and since 2001, the Dean of the School of Life Science and Technology of UESTC. He had been a Visiting Scholar at University of Illinois at Chicago, from September 1997 to August 1998, and a Visiting Professor at McMaster University, Hamilton, ON, Canada, from November 2000 to May 2001, and at Aalborg University, Aalborg, Denmark, from November 2003 to February 2004. He is the author or coauthor of more 80 papers and 5 books. His current interests include EEG, fMRI and their applications in cognitive science and neurological problems

Lin Chen is an Academician of Chinese Academy of Science, and the director of the Key Laboratory of Cognitive Science, Graduate School and Institute of Biophysics, Chinese Academy of Science, Beijing, China. His major contribution is the theory of topological perception with two papers published by Science in 1982 and 2003. His major research interests include perception theory and fMRI, EEG and MEG

Wufan Chen is a Professor at the Southern Medical University, Guangzhou, China. He is the PI of a National 973 Project. He is the author or coauthor of more 100 papers and has received more than five awards from the GuangDong Province or PLA, China. His research interests include biomedical imaging and image processing.